Voltage-Driven Nonlinearity in Magnetoelectric Heterostructures

Zhaoqiang Chu,[1,2,*] Cunzheng Dong,[1] Cheng Tu,[1,3,†] Yifan He,[1] Xianfeng Liang,[1] Jiawei Wang,[1,4] Yuyi Wei,[1] Huaihao Chen,[1] Xiangyu Gao,[2] Caijiang Lu,[1] Zengtai Zhu,[1] Yuanhua Lin,[5] Shuxiang Dong,[2,6,‡] Jeffrey McCord,[7] and Nian-Xiang Sun[1,§]

[1] *Department of Electrical and Computer Engineering, Northeastern University, Boston, Massachusetts 02115, USA*

[2] *College of Engineering, Peking University, Beijing 100871, China*

[3] *School of Electronic Science and Engineering, University of Electronic Science and Technology of China, Chengdu, 611731, China*

[4] *College of Science, Zhejiang University of Technology, Hangzhou 310023, China*

[5] *School of Materials Science and Engineering, Tsinghua University, Beijing, China*

[6] *Beijing Key Laboratory for Magnetoelectric Materials and Devices (BKL-MEMD), Peking University, 100871 Beijing, China*

[7] *Institute for Materials Science, Kiel University, Kaiserstraße 2, 24143 Kiel, Germany*

(Received 23 June 2019; published 1 October 2019)

Magnetoelectric (ME) heterostructures are widely studied to realize functional applications, such as magnetometers, ME random access memory (MERAM), ME antennas, energy harvesters, and voltage microwave devices. A good understanding of the nonlinearity of ME heterostructures can lead to potentially improved performance. Here, we present an investigation into the voltage-driven nonlinear phenomena of a ME heterostructure near its electromechanical resonance. The Stoner-Wohlfarth model and Duffing equation are used to study the ΔE effect in amorphous Metglas alloy and the nonlinear behavior of a ME heterostructure, respectively. Then, the dependence of the nonlinearity on bias field, driving voltage, mechanical quality factor, and the frequency sweeping direction are systematically studied and verified. Experimental results show that spring-hardening and -softening behavior is separately obtained at bias fields of 25 Oe and 50 Oe, respectively. In addition, hysteresis is observed when sweeping the frequency forward and then backward at a driving voltage of 5 V; this agrees well with qualitative analysis. This work provides a route to induce, control, and possibly exploit the nonlinear behavior of ME devices, such as magnetic-field energy harvesters and ME sensors and antennas.

DOI: 10.1103/PhysRevApplied.12.044001

I. INTRODUCTION

Investigations into the magnetoelectric (ME) coupling effect, which enables interactions between magnetization and polarization in single-phase or composite materials, have made enormous progress and provide diverse routes to new functional device architectures, including ME random access memory (MERAM) [1], sensors [2–5], energy harvesters [6–8], microwave devices [9–11], and recently proposed very low frequency (VLF) ME antenna [12–15]. While several ME coupling mechanisms have been proposed over the past few decades, strain-mediated manipulation is, in general, the most promising one [4,10,16]. Compared with single-phase ME materials, ME heterostructures feature much higher coupling capacity [4]. For instance, Liu *et al.* realized giant electric field tuning of magnetic properties in $Fe_3O_4/Pb(Mg_{2/3}\text{-}Nb_{1/3})O_3\text{-}PbTiO_3$(PMN-PT) heterostructure based on the converse ME (CME) effect [17]. Chu *et al.* reported a (1-1)-type laminate using the direct ME (DME) effect, which exhibited an enhanced ME coefficient of 7000 V cm^{-1} Oe^{-1} [18].

With respect to functional devices based on the strain-mediated DME effect, the strain generated in a piezomagnetic layer is normally limited to low amplitude due to the low saturated magnetostriction coefficient and small driving ac magnetic field [4,18,19]. In this regard, we can safely deal with the vibration system with linear elastic theory, even under resonance conditions. Notably, here the linearity issue is related only to the Young's modulus of the system; however, the widely reported nonlinear ME effect, which mainly considers the nonlinear magnetostriction coefficient, is not within the scope of

*zhaoqiangchu@pku.edu.cn
†ctu@uestc.edu.cn
‡sxdong@pku.edu.cn
§n.sun@northeastern.edu

this work [20–23]. A completely different situation will occur when we are studying the strain-mediated CME effect [10,24]. In this case, a large strain electrically excited in the piezoelectric layer is desired, to effectively manipulate magnetic properties in magnetoelectric heterostructures [25–29]. For example, a high static electric field (normally higher than 2 kV/cm) is expected to induce an obvious change of ferromagnetic resonance frequency in (Fe, Ga)B/PZN − PT multiferroic heterostructures [30]. Large strain or a high electric field are not a problem in the case of quasi-static manipulation, if the piezoelectric material is physically and electrically safe.

Different from the ME heterostructure, which operates under quasi-static control, resonant ME devices based on the converse ME effect will face frequency-response nonlinearity issues under a high vibrational amplitude. Over the last few years, the concept of strain-powered antennas based on magnetoelectric or single piezoelectric effects has been proposed to realize VLF antennas, which work under resonance conditions and are typically used in circumstances such as underground communications and through-building communications [12,14,16,31–33]. In 2017, for example, an acoustically actuated nanoelectromechanical system (NEMS) ME antenna with a compact size was first proposed with the aim of antenna miniaturization [34]. In 2019, Xu *et al.* reported a VLF ME antenna that exhibited much higher efficiency, as compared to a current-loop antenna of the same size [12]. Conceptually, this VLF antenna based on a ME heterostructure uses the CME effect, but works under resonance conditions [12]. To realize a long communication distance, a higher input power, which produces much larger vibrational amplitude and coupling stress, will be favorable as a general practice [12]. For widely used ferromagnetic materials, such as Metglas and Terfenol-D, it is known that their Young's moduli will change dramatically in response to external stress and magnetic field; this is termed the Delta-E effect [35–37]. In this regard, the ME antenna is now a nonlinear vibration system from the perspective of mechanics. Thus, nonlinearity might serve to further improve the ME antenna's performances, as discussed in Sec. III.

However, very few theoretical or experimental papers have reported nonlinearity in the ME heterostructure that operates under resonance conditions and has a high-field input. Here, we present a fundamental discussion concerning the nonlinear phenomenon in the converse ME effect. The ME heterostructure consists of a $Pb(Mg_{2/3}\text{-}Nb_{1/3})O_3\text{-}Pb(Zr, Ti)O_3$ crystal (PMN-PZT) and amorphous (Fe, B)Si alloy (Metglas) working in longitudinal-transverse (L-T) mode. Functioning as a ME antenna, a coil receiver or a pick-up coil is used to detect the varied magnetization of the magnetic layer through the CME effect. The Delta-E effect of Metglas is demonstrated with a simplified Stoner-Wohlfarth model and the exemplary Duffing equation is then utilized to analyze the simplified nonlinear system. The dependence of nonlinearity on magnetic bias field, input voltage, mechanical quality factor (Q_m) and frequency-sweeping orientation is studied experimentally. Spring-hardening and -softening resonance and jumping phenomenon in frequency-response are both observed. We believe this work provides perspectives for either limiting or exploiting nonlinearity, especially for the ME antenna in future work.

II. EXPERIMENTS AND FUNDAMENTALS

Figure 1(a) schematically presents the ME heterostructure (acting as a ME antenna) and the pick-up coil (acting as a receiver). The core of the ME heterostructure is a thickness-poled PMN-PZT crystal with the sizes of $30 \times 1 \times 0.2$ mm^3 (Ceracomp Co., Ltd.), of which on the top and bottom sides are five-layered Metglas fibers with sizes of $52 \times 1.5 \times 0.125$ mm^3. The piezoelectric and piezomagnetic fibers are well bonded together with epoxy resin to finally form a ME heterostructure with a similar structure to that of (1-1) ME composites, which feature a high mechanical quality factor and DME coupling coefficient, as demonstrated in our previous studies [5,18]. Here, the ME heterostructure working on the CME effect can be understood as an ME antenna and a homemade pick-up coil is used to capture the output magnetic signal. Notably, nonlinearity generally exists in a ME resonator, but is not limited to ME antennas. The excitation voltage to drive the PMN-PZT crystal and the output voltage of the pick-up coil are separately generated and obtained by one lock-in amplifier (SR830, Stanford Research, USA). The bias field, H_{dc}, is provided by a commercial Helmholtz coil system. Both stress and bias field are applied along the long axis of the ME antenna. In work by Xu *et al.*, the pick-up coil was placed 40 cm along the longitudinal direction of the ME antenna [12]. Since the communication distance is not the topic in this work, we simply ignore the distance and place the ME heterostructure inside the coil, as shown in Fig. 1(a), to study the nonlinearity issue.

In 1990, Squire proposed a phenomenological model for the Delta-E effect in field-annealed amorphous ribbons (Metglas) by taking into account the domain wall movement and multidomain rotation [37]. To simplify this model, we qualitatively analyze the Delta-E effect in Metglas, without considering the domain walls, and the calculated results basically agree with a typical experimental profile. For transversely annealed amorphous ribbons, the initial easy axis is basically along the width direction ($K_\perp$) and the longitudinal magnetostriction coefficient can be maximized in this case, but inevitable internal stress can tilt the initial moment direction (M_0), to some extent [36]. The original domain pattern of Metglas in a demagnetized state is shown in Fig. 1(b), as captured by MOKE

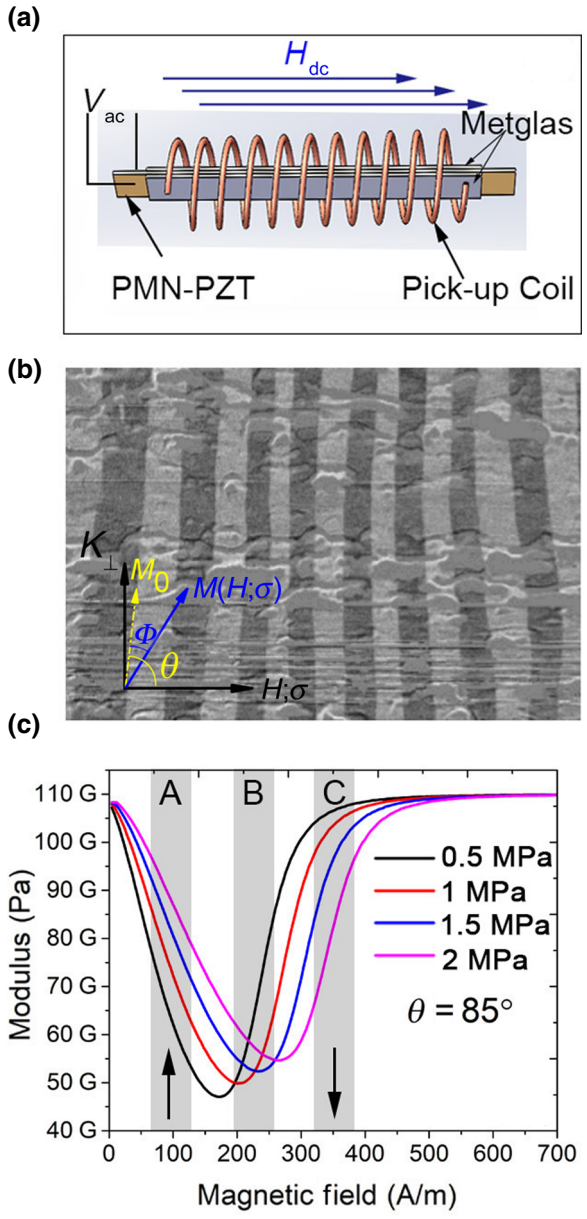

FIG. 1. (a) Schematic of the ME heterostructure incorporating Metglas as magnetostrictive phase and PMN-PZT crystals as piezoelectric phase. A sine voltage is used to drive the sample and a pick up is utilized to capture the induced signal. (b) The magnetic domain patter in the amorphous alloy Metglas is obtained by magneto-optic Kerr effect (MOKE) microscopy. The average width of the magnetic domain is 120 μm. (c) The calculated Young's modulus of Metglas as a function of the applied magnetic field and stress along the long axis with $K_\perp = 100$ J/m^3, $\mu_0 M_s = 1.2$ T, $\lambda_s = 27$ ppm, $\theta = 85°$ and $E_s = 110$ GPa.

microscopy [38]. M_0 makes an angle of $\theta = 85°$ with the ribbon longitudinal axis. The magnetization is aligned nearly perpendicular to the length of the ribbon. When the magnetization moment is subjected to the external field and stress, the total energy, U, is [37]:

$$U = K_\perp \sin^2\Phi - \mu_0 M_s H\cos(\theta - \Phi) + \frac{3}{2}\lambda_s\sigma\sin^2(\theta - \Phi), \tag{1}$$

where Φ, which is determined by the energy-minimizing rule, is the angle between the magnetization direction $M(H,\sigma)$ and initial moment direction (M_0); H and σ are applied magnetic field and stress, respectively; $K_\perp$, M_s, and λ_s are the transverse anisotropy constant, saturation magnetization, and saturation magnetostriction, respectively. Different from ordinary linear elastic materials, the longitudinal strain, ϵ, here is the sum of elastic strain, ϵ_s, and magnetic strain, ϵ_H [36,37]:

$$\varepsilon = \underbrace{\frac{\sigma}{E_s}}_{\varepsilon_s} + \underbrace{\frac{3}{2}\lambda_s\sigma\sin^2(\theta - \Phi)}_{\varepsilon_H}. \tag{2}$$

Based on the definition of the material's modulus, we have [36]:

$$\frac{1}{E} = \frac{\partial\varepsilon}{\partial\sigma} = \frac{1}{E_s} + \frac{\partial\varepsilon_H}{\partial\sigma} = \frac{1}{E_s} + \frac{9}{8}\frac{\lambda_s^2}{K_\perp} \times \left\{\frac{\sin^2 2(\theta - \Phi)}{\cos 2\Phi + \frac{\mu_0 M_s H}{2K_\perp}\cos(\theta - \Phi) + \frac{3\lambda_s\sigma}{2K_\perp}\cos 2(\theta - \Phi)}\right\}, \tag{3}$$

where E_s is the saturation modulus. Figure 1(c) gives the calculated results, according to Eqs. (1)–(3). Considering the model simplification, Fig. 1(c) can be viewed only as an exemplary and qualitative analysis to capture the dependence of the Delta-E effect on applied stress and magnetic field. Three highlighted regions, labeled A, B, and C, suggest three typical changing behaviors of the material's modulus in response to external stress. In region A, with a bias field of around 100 A/m, the material's Young's modulus, E, increases as the compressive stress increases from 0.5 MPa to 2 MPa, while the trend is opposite in region C, with a larger bias field of around 300 A/m. In region B, E fluctuates slightly. In a linear vibration system, the Young's modulus is basically assumed to be constant. The result given in Fig. 1(c) naturally implies the existence of nonlinear behavior occurring in a Metglas-based resonator and a strong magnetic field dependence of this kind of behavior.

The vibration behavior of ME resonators with a nonlinear spring constant due to the ΔE effect is then modeled as a forced single degree-of-freedom (DOF) system, of which the displacement, μ, governing equation is typically described with the Duffing equation [39,40]:

$$m\ddot{u} + c\dot{u} + k_1\mu + k_3\mu^3 = F\cos(\omega t), \tag{4}$$

where m is the equivalent mass; c is the total damping constant, which can be expressed as $1/(2Q_m)$, with Q_m as the mechanical quality factor; $F\cos(\omega t)$ is the effective driving force based on a piezoelectric effect with an angular frequency of ω; k_1 and k_3 are the linear and cubic spring constants, respectively (here we use $k = k_1 + k_3\mu^2$ to roughly describe the ΔE effect). Since the maximum driving voltage (5 V, corresponding to a field of 0.25 kV/cm) used in this work is far lower than the coercive field, E_C (2 kV/cm), of PMN-PZT, the piezoelectric phase is considered to be linear; its piezoelectric constants are attributed to the intrinsic contribution and reversible domain wall motion [41]. For a qualitative understanding of the nonlinear issue, Fig. 2(a) first gives the frequency response of the vibration displacement with typical parameters (see Table S2 in the Supplemental Material [42]) by solving Eq. (4). As shown in Fig. 2(a), a linear, and thus, symmetric, resonance peak is obtained when the nonlinear spring constant $k_3 = 0$. A negative $k_3 = -100 \times 10^9$ N/m^3 leads the resonance peak bending toward the left, while positive $k_3 = 100 \times 10^9$ N/m^3 gives rise to bending toward the right. Two highlighted regions in Fig. 2(a) indicate that the analytical solution from point A to point C and from point E to point G is unstable and unreachable experimentally. Therefore, a jumping phenomenon and a hysteresis loop can be generated when sweeping the frequency forward and backward. Specifically, the displacement will jump down first from point C to point D with forward frequency sweeping and jump up from point A to point B when the frequency sweeps back in a hardening system with $k_3 > 0$. Such a hysteresis loop has been widely used to enlarge the -3 dB bandwidth of vibration energy harvesters [45,46]. This bandwidth improvement may also allow higher data bit rates with respect to a ME antenna based on Shannon's formula [31,47].

Regarding such a nonlinear system, the natural frequency, ω_0, is controlled by $\sqrt{k_1/m}$. The nonlinear spring constant, k_3, is certainly the key parameter that determines the final mechanical behavior. However, the total damping, c (or Q_m), and level of driving force F play important roles as well. When we keep Q_m and k_3 at 100 and 100×10^9 N/m^3, respectively, it is clearly shown in Fig. 2(b) that the decrease in the driving force F will weaken and finally eliminate the nonlinear behavior, as the amplitude of the driving force goes from 0.5 N down to 0.1 N. Decreasing the value of Q_m works similarly, as presented in Fig. 2(c). Based on this quantitative analysis, the nonlinear spring constant, damping coefficient, and driving amplitude jointly shape the frequency-response characteristics of a ME heterostructure. Notably, nonlinear behavior can be strongly suppressed, even though the ΔE effect is obvious in Metglas, when the mechanical quality factor and driving force are normally low. The following experimental results systematically demonstrate nonlinearity generation and control in a ME heterostructure.

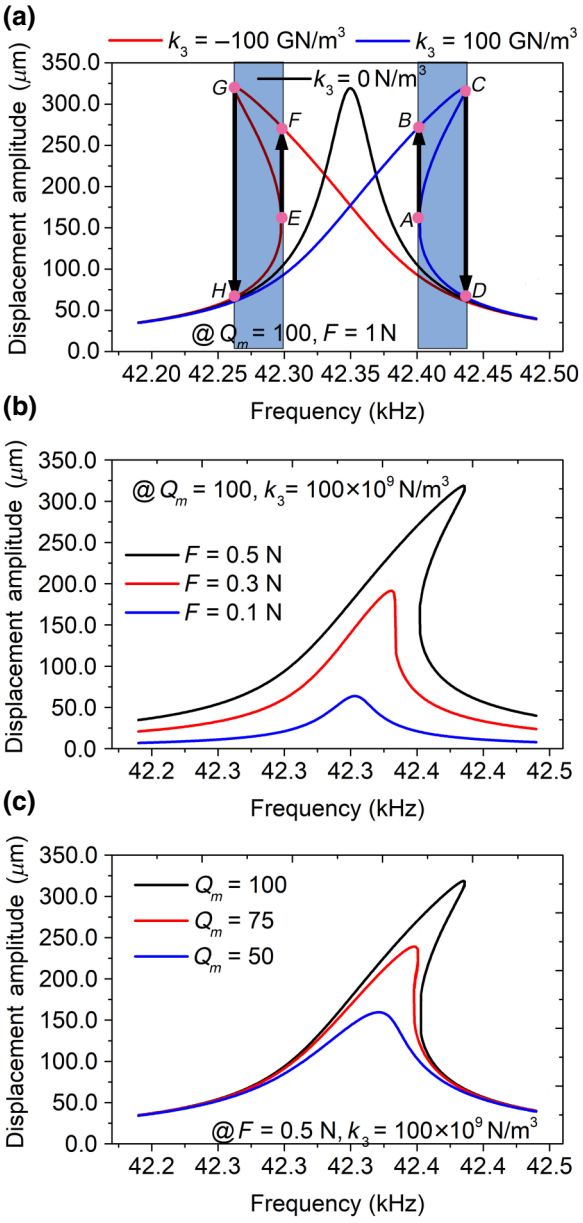

FIG. 2. (a) Exemplary frequency response of the displacement amplitude for a nonlinear system with $k_3 = -100 \times 10^9$, 0, and 100×10^9 N/m^3. The effective mass, m, and the linear spring constant are 22.62 mg and 1.6×10^6 N/m, respectively. Q and driving force are kept as 100 and 1 N, respectively. The dependence of (b) the driving force, F (=0.5 N, 0.3 N, 0.1 N), and (c) Q_m (=100, 75, 50) on the nonlinearity.

III. RESULTS AND DISCUSSION

As observed in Fig. 1(c), the intensity of the bias field can change the level and sign of the nonlinear spring constant, k_3; therefore, inducing completely different nonlinear behavior, as presented in Fig. 2(a). We first obtain the frequency response of the induced voltage from the pick-up coil, within which a change of the magnetic flux is generated due to the periodic change of magnetization, which

is controlled by piezoelectric stress [48]. We assume the change in behavior of the magnetization can be reflected in the vibrational profile of the nonlinear system, which means the qualitative result in Fig. 2 provides a reference for the nonlinear frequency response of the induced voltage. The frequency response of the induced voltage with a bias field, H_{dc}, varying from 2 Oe to 60 Oe is presented in Figure S1 in the Supplemental Material [42]. Figure 3(a) compares three kinds of typical results, corresponding to bias fields of 20 Oe, 35 Oe, and 50 Oe, through forward sweeping of the driving frequency, but with a fixed driving voltage of 5 V. At a bias field of 20 Oe, a prominent spring-hardening resonance is observed, with the resonance voltage sharply jumping down after reaching the peak point. Agreeing well with the discussion of the ΔE effect, as shown in Fig. 1(c), a spring-softening resonance is then generated once the bias field increases to a higher value, e.g., 50 Oe, as shown in Fig. 3(a), while the system is almost linear when the bias field lies in an intermediate value, e.g., 35 Oe. As shown in Fig. 2(b), a decrease in the driving force F will weaken and finally eliminate the nonlinear behavior. This is tested and verified by our experimental results, as presented in Fig. 3(b). It is clear that the spring-hardening phenomenon occurs at a bias field of 20 Oe, as shown in Fig. 3(a), and gradually disappears when the driving voltage decreases from 5 V to 1 V.

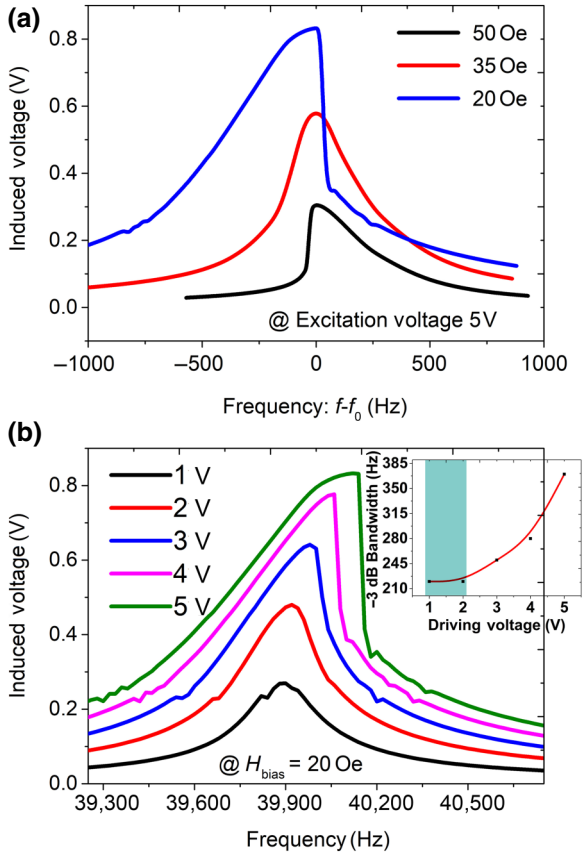

FIG. 3. (a) Measured frequency response of the induced voltage under different bias fields for the ME heterostructure. The x axis is the expressed as a frequency offset with respect to the center frequency, f_0. (b) Measured frequency response of the induced voltage under driving voltages from 1 V to 5 V at a fixed bias field of 20 Oe. The inset of Fig. 3(b) gives the corresponding −3 dB bandwidth values.

In work by Xu *et al.* [12], an input voltage of 10 V was used to excite the VLF ME antenna. To further increase the transmitted magnetic field intensity, and thereby increase the communication distance, a high input voltage level is required. In this regard, nonlinearity can notably affect the antenna transmitting performance and care should be taken. For instance, we should synchronously change the driving frequency to ensure a maximum signal output as the resonance point gradually shifts toward the left, as shown in Fig. 3(b). In addition, the −3 dB bandwidth of the antenna transmitting characteristic is calculated as given in the inset of Fig. 3(b). A linear system with a driving voltage of 1 V or 2 V has an unchanged −3 dB bandwidth of 220 Hz, while a nonlinear system with a driving voltage ranging from 3 V to 5 V exhibits an increasing −3 dB bandwidth of up to 370 Hz under 5 V excitation. For a potential ME antenna communication system, data bit rate, which is normally limited by system bandwidth, is also of significance. Recently, Kemp *et al.* reported a strain-powered VLF transmitter with a high Q_m and a high modulation rate through the frequency shift keying (FSK) modulation method [31]. Due to the extremely low bandwidth of the high Q_m resonator system, direct antenna modulation (DAM), by controlling an assisted capacitor to vary the mechanical resonance frequency, is additionally used to implement the FSK coding. Here, we believe that nonlinearity can result in a promising performance enhancement on antenna modulation, in terms of the data rate, through a higher bandwidth, and operation complexity, through spontaneous signal-mixing performance [49,50].

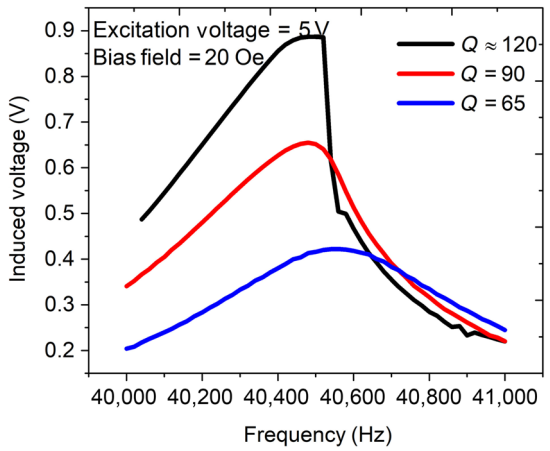

FIG. 4. Measured frequency response of the induced voltage under different Q factors for the ME heterostructure.

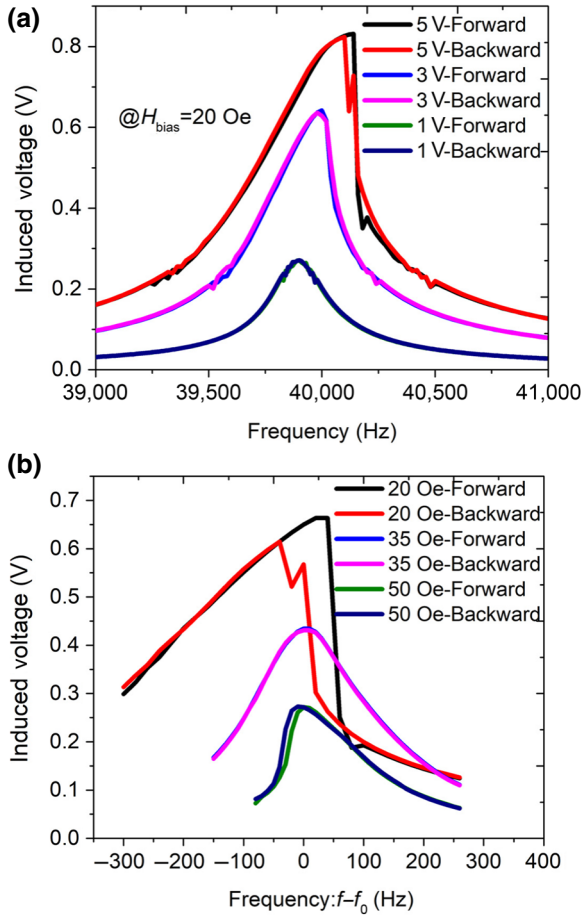

FIG. 5. (a) Measured frequency response of the induced voltage under different driving voltages at a fixed bias field of 20 Oe for the ME heterostructure. Here, the driving voltage is applied by forward and backward sweeping of the frequency. (b) Measured frequency response of the induced voltage under different bias fields, but at a fixed voltage of 5 V for the (1-1) ME sensor. The (1-1) ME sensor consists of a thickness-poled [011]-oriented PMN-PZT fiber with sizes of $30 \times 1 \times 0.2$ mm^3 and five-layered Metglas fibers with sizes of $100 \times 1.5 \times 0.125$ mm^3 bonded on the bottom and top sides of the piezoelectric phase.

Then we test the dependence of the nonlinear behaviour on Q_m for our ME heterostructure, as shown in Fig. 4. In order not to influence the vibration mode, but only change the Q_m of the system, we choose to vary the suspension area near the node position that supports the whole structure. With a minimum suspension area, the Q_m is around 120 and successfully leads to a spring-hardening behaviour. An accurate calculation of Q_m based on the nonlinear resonance curve is not available. However, when enlarging the suspension area, and thus, decreasing Q_m to 65, the nonlinear behaviour is gradually weakened and then completely disappears, as shown in Fig. 4. Naturally, decreasing Q_m gives rise to a corresponding decrease in the generated magnetic field signal, and thereby, the induced voltage. High Q_m is strongly desired for a low-loss ME antenna. In this regard, nonlinearity may be inevitable when we are further designing and operating a ME antenna in the future.

As shown in Fig. 3(a), a hysteresis loop can be generated when sweeping the frequency forward and backward for a nonlinear system, which is used to realize dynamic state switching for memory or logic device designs [51]. Thus, we try to excite such a hysteresis loop for our ME heterostructure. As shown in Fig. 5(a), the bias field is fixed at 20 Oe. Under a small driving voltage of 1 V, linear behavior is excited and we do not observe any sign of a hysteresis loop. When increasing the driving voltage to 3 V, a slightly asymmetric resonance curve is induced, but the nonlinearity is still not strong enough to generate an obvious hysteresis loop. Finally, we observe that the hysteretic phenomenon is going to occur as the driving voltage is increased to 5 V, as depicted in Fig. 5(a). Although the jumping phenomenon is clear, the hysteresis loop is not as big as that theoretically presented in Fig. 2(a). We then further conduct a bidirectional frequency sweeping experiment using the (1-1)-type ME sensor that we have reported previously [18]. Since (i) the mechanical quality factor and ME coupling coefficient are much higher and (ii) the volume fraction of Metglas is enlarged for a (1-1) ME sensor, with a Metglas fiber of 100 mm in length, but maintaining the dimension of the piezoelectric phase, the Q_m- and k_3-related nonlinearity can be increased. As expected, at a bias field of 20 Oe, a strong hardening resonance is induced and a prominent hysteresis loop appears, as shown in Fig. 5(b). Basically, agreeing well with the results in Fig. 3(a), linear and softening resonances are also generated at bias fields of 35 Oe and 50 Oe, respectively. Although the nonlinear behavior can increase the bandwidth of the resonator system, and thus, allow an easier FSK scheme or increased data bit rates, it is evident that a large hysteresis should be treated cautiously, or even be avoided, for a stable amplitude output with respect to the FSK scheme [31].

IV. CONCLUSION

In summary, we investigate the nonlinearity in a ME heterostructure in this work. Due to the large ΔE effect in amorphous Metglas alloy, a ME resonator can be a natural nonlinear system. A strong magnetic field dependence of the nonlinear behavior (resonance hardening and softening) is presented. The Stoner-Wohlfarth model is used to describe changes to the Metglas Young's modulus. Equivalent to a mass-spring-damper system with a single DOF, the nonlinear behavior of the ME antenna is qualitatively studied using a typical Duffing equation. Experimental results show spring-hardening and -softening resonance and a hysteresis loop in frequency-response of the induced voltage from the pick-up coil are both successfully observed. The theoretical analysis also agrees well with experimental results. In particular, both high Q

and high driving voltage, along with a nonlinear spring constant, k_3, are critical factors to induce nonlinear behavior in a ME heterostructure. In contrast to a conventional microresonator, a new controllable variable, e.g., magnetic field, is introduced. Regarding the nonlinearity itself, a more accurate theoretical and experimental method to determine the nonlinear spring constant, k_3, of the studied system may also be of interest to the mechanics community.

From the perspective of applications, the ME heterostructure is studied as a strain-powered VLF antenna in this work. By systematically studying the functions of bias magnetic field, driving voltage, mechanical quality factor, and frequency sweeping direction on the nonlinearity, we also provide a route to induce, control, and possibly exploit the nonlinear behavior of ME devices. Particularly, the effect of the nonlinear behavior on a ME antenna's communication distance, bandwidth, and modulation scheme is preliminarily discussed. In addition, notably, nonlinearity generally exists in a ME resonator, but is not limited to ME antennas, and we believe this fundamental work will open up a new dimension for the design and operation of such resonant ME devices in the future.

ACKNOWLEDGMENTS

This work is supported by the National Natural Science Foundation of China (Grants No. 51132001, No. 51072003, No. 51729201, and No. 51772005) and China Scholarship Council (Grant No. 201806010294).

[1] X. Chen, A. Hochstrat, P. Borisov, and W. Kleemann, Magnetoelectric exchange bias systems in spintronics, Appl. Phys. Lett. **89**, 202508 (2006).

[2] N. A. Spaldin and R. Ramesh, Advances in magnetoelectric multiferroics, Nat. Mater. **18**, 203 (2019).

[3] D. Viehland, M. Wuttig, J. McCord, and E. Quandt, Magnetoelectric magnetic field sensors, MRS Bull. **43**, 834 (2018).

[4] Z. Chu, M. PourhosseiniAsl, and S. Dong, Review of multilayered magnetoelectric composite materials and devices applications, J. Phys. D Appl. Phys. **51**, 243001 (2018).

[5] Z. Chu, W. Shi, H. Shi, Q. Chen, L. Wang, M. J. PourhosseiniAsl, C. Xiao, T. Xie, and S. Dong, A 1D magnetoelectric sensor array for magnetic sketching, Adv. Mater. Technol. **4**, 1800484 (2018).

[6] Z. Chu, V. Annapureddy, M. PourhosseiniAsl, H. Palneedi, J. Ryu, and S. Dong, Dual-stimulus magnetoelectric energy harvesting, MRS Bull. **43**, 199 (2018).

[7] C. M. Leung, J. Li, D. Viehland, and X. Zhuang, A review on applications of magnetoelectric composites: from heterostructural uncooled magnetic sensors, energy harvesters to highly efficient power converters, J. Phys. D Appl. Phys. **51**, 263002 (2018).

[8] V. Annapureddy, H. Palneedi, G.-T. Hwang, M. Peddigari, D.-Y. Jeong, W.-H. Yoon, K.-H. Kim, and J. Ryu, Magnetic energy harvesting with magnetoelectrics: an emerging technology for self-powered autonomous systems, Sustainable Energy Fuels **1**, 2039 (2017).

[9] J. Domann, T. Wu, T.-K. Chung, and G. Carman, Strain-mediated magnetoelectric storage, transmission, and processing: Putting the squeeze on data, MRS Bull. **43**, 848 (2018).

[10] A. Molinari, H. Hahn, and R. Kruk, Voltage-control of magnetism in all-solid-state and solid/liquid magnetoelectric composites, Adv. Mater. **31**, 1806662 (2019).

[11] H.-X. Zou, W.-M. Zhang, W.-B. Li, K.-M. Hu, K.-X. Wei, Z.-K. Peng, and G. Meng, A broadband compressive-mode vibration energy harvester enhanced by magnetic force intervention approach, Appl. Phys. Lett. **110**, 163904 (2017).

[12] J. Xu, C. M. Leung, X. Zhuang, J. Li, S. Bhardwaj, J. Volakis, and D. Viehland, A low frequency mechanical transmitter based on magnetoelectric heterostructures operated at their resonance frequency, Sensors (Basel) **19**, 853 (2019).

[13] J. P. Domann and G. P. Carman, Strain powered antennas, J. Appl. Phys. **121**, 044905 (2017).

[14] H. Lin, M. R. Page, M. McConney, J. Jones, B. Howe, and N. X. Sun, Integrated magnetoelectric devices: Filters, pico-Tesla magnetometers, and ultracompact acoustic antennas, MRS Bull. **43**, 841 (2018).

[15] M. Fechner, N. A. Spaldin, and I. E. Dzyaloshinskii, Magnetic field generated by a charge in a uniaxial magnetoelectric material, Phys. Rev. B **89**, 184415 (2014).

[16] H. Palneedi, V. Annapureddy, S. Priya, and J. Ryu, Status and perspectives of multiferroic magnetoelectric composite materials and applications, Actuators **5**, 9 (2016).

[17] M. Liu *et al.*, Giant electric field tuning of magnetic properties in multiferroic ferrite/ferroelectric heterostructures, Adv. Funct. Mater. **19**, 1826 (2009).

[18] Z. Chu, H. Shi, W. Shi, G. Liu, J. Wu, J. Yang, and S. Dong, Enhanced resonance magnetoelectric coupling in (1-1) connectivity composites, Adv. Mater. **29**, 1606022 (2017).

[19] Y. Wang, D. Gray, D. Berry, J. Gao, M. Li, J. Li, and D. Viehland, An extremely low equivalent magnetic noise magnetoelectric sensor, Adv. Mater. **23**, 4111 (2011).

[20] M. Li, C. Dong, H. Zhou, Z. Wang, X. Wang, X. Liang, Y. Lin, and N. X. Sun, Highly sensitive DC magnetic field sensor based on nonlinear ME effect, IEEE Sens. Lett. **1**, 1 (2017).

[21] R. Jahns, H. Greve, E. Woltermann, E. Quandt, and R. Knöchel, Sensitivity enhancement of magnetoelectric sensors through frequency-conversion, Sens. Actuators, A **183**, 16 (2012).

[22] Z. Chu, Z. Yu, M. PourhosseiniAsl, C. Tu, and S. Dong, Enhanced low-frequency magnetic field sensitivity in magnetoelectric composite with amplitude modulation method, Appl. Phys. Lett. **114**, 132901 (2019).

[23] H.-M. Zhou, M.-H. Li, Y. Zhou, and Q. Chen, Nonlinear resonant magnetoelectric coupling model for dual-peak phenomenon in magnetoelectric laminates, J. Alloys Compd. **672**, 292 (2016).

[24] P. Zhou *et al.*, Converse magnetoelectric effects in composites of liquid phase epitaxy grown nickel zinc ferrite

films and lead zirconate titanate: Studies on the influence of ferrite film parameters, Phys. Rev. Mater. **3**, 044403 (2019).

[25] Y. Sun *et al.*, Electric-field modulation of interface magnetic anisotropy and spin reorientation transition in (Co/Pt)3/PMN-PT heterostructure, ACS Appl. Mater. Interfaces **9**, 10855 (2017).

[26] F. Matsukura, Y. Tokura, and H. Ohno, Control of magnetism by electric fields, Nat. Nanotechnol. **10**, 209 (2015).

[27] Z. Hu, T. Nan, X. Wang, M. Staruch, Y. Gao, P. Finkel, and N. X. Sun, Voltage control of magnetism in FeGaB/PIN-PMN-PT multiferroic heterostructures for high-power and high-temperature applications, Appl. Phys. Lett. **106**, 022901 (2015).

[28] J. Lou, D. Reed, M. Liu, and N. X. Sun, Electrostatically tunable magnetoelectric inductors with large inductance tunability, Appl. Phys. Lett. **94**, 112508 (2009).

[29] T. Nan, J. M. Hu, M. Dai, S. Emori, X. Wang, Z. Hu, A. Matyushov, L. Q. Chen, and N. Sun, A strain-mediated magnetoelectric-spin-torque hybrid structure, Adv. Funct. Mater. **29**, 1806371 (2018).

[30] J. Lou, M. Liu, D. Reed, Y. Ren, and N. X. Sun, Giant electric field tuning of magnetism in novel multiferroic FeGaB/lead zinc niobate-lead titanate (PZN-PT) heterostructures, Adv. Mater. **21**, 4711 (2009).

[31] M. A. Kemp, M. Franzi, A. Haase, E. Jongewaard, M. T. Whittaker, M. Kirkpatrick, and R. Sparr, A high Q piezoelectric resonator as a portable VLF transmitter, Nat. Commun. **10**, 1715 (2019).

[32] J. A. Bickford, A. E. Duwel, M. S. Weinberg, R. S. McNabb, D. K. Freeman, and P. A. Ward, Performance of electrically small conventional and mechanical antennas, IEEE Trans. Antennas Propag. **67**, 2209 (2019).

[33] Yiming Liu, Jesse Simon, Robert C. O'Handley, and Jiankang Huang, *Wirelesstransfer Of Information Using Magneto-Electric Devices* (Burlington, 2009).

[34] T. Nan *et al.*, Acoustically actuated ultra-compact NEMS magnetoelectric antennas, Nat. Commun. **8**, 296 (2017).

[35] X. J. Zheng and X. E. Liu, A nonlinear constitutive model for Terfenol-D rods, J. Appl. Phys. **97**, 053901 (2005).

[36] D. Y. Kim, C. G. Kim, H. C. Kim, and U. H. Sung, Stress dependence of ΔE in amorphous ribbon, J. Appl. Phys. **81**, 5811 (1997).

[37] P. T. Squire, Phenomenological model for magnetization, magnetostriction and Ae effect in field-annealed amorphous ribbons, J. Magn. Magn. Mater. **87**, 299 (1990).

[38] J. McCord, Progress in magnetic domain observation by advanced magneto-optical microscopy, J. Phys. D Appl. Phys. **48**, 333001 (2015).

[39] S. Neiss, F. Goldschmidtboeing, M. Kroener, and P. Woias, Analytical model for nonlinear piezoelectric energy harvesting devices, Smart Mater. Struct. **23**, 105031 (2014).

[40] V. Kaajakari, T. Mattila, A. Oja, and H. Seppa, Nonlinear limits for single-crystal silicon microresonators, J. Microelectromech. Syst. **13**, 715 (2004).

[41] F. Li and S. Zhang, High performance ferroelectric relaxorPbTiO3 single crystals: Status and perspective, J. Appl. Phys. **111**, 031301 (2012).

[42] See Supplemental Material at http://link.aps.org/supplemental/10.1103/PhysRevApplied.12.044001, which includes Ref. [43,44], for a measured frequency response of the induced voltage under different bias fields for the ME heterostructure and a demonstration of the spring-mass-damper model to obtain the equivalent mechanical parameters.

[43] K. S. Tran, H. V. Phan, H. Y. Lee, Y. Kim, and H. C. Park, Blocking force of a piezoelectric stack actuator made of single crystal layers (PMN-29PT), Smart Mater. Struct. **25**, 095038 (2016).

[44] V. T. Dau and T. X. Dinh, Numerical study and experimental validation of a valveless piezoelectric air blower for fluidic applications, Sens. Actuators, B **221**, 1077 (2015).

[45] F. Cottone, H. Vocca, and L. Gammaitoni, Nonlinear Energy Harvesting, Phys. Rev. Lett. **102**, 080601 (2009).

[46] Z. Lin, J. Chen, X. Li, J. Li, J. Liu, Q. Awais, and J. Yang, Broadband and three-dimensional vibration energy harvesting by a non-linear magnetoelectric generator, Appl. Phys. Lett. **109**, 253903 (2016).

[47] K. C. D. I. J. Good, A paradox concerning rate of information, Inf. Control **1**, 113 (1958).

[48] P. Hayes, V. Schell, S. Salzer, D. Burdin, E. Yarar, A. Piorra, R. Knöchel, Y. K. Fetisov, and E. Quandt, Electrically modulated magnetoelectric AlN/FeCoSiB film composites for DC magnetic field sensing, J. Phys. D Appl. Phys. **51**, 354002 (2018).

[49] C. E. Shannon, Communication in the presence of noise, Proc. IEEE **72**, 1192 (1949).

[50] W. Yao and Y. Wang, Direct antenna modulation - a promise for ultra-wideband (UWB) transmitting, IEEE MTI-S Int. Microw. Symp. Dig. **2**, 1273 (2004).

[51] T.-D. Onuta, Y. Wang, C. J. Long, S. E. Lofland, and I. Takeuchi, Dynamic state switching in nonlinear multiferroic cantilevers, Appl. Phys. Lett. **101**, 043506 (2012).